JAAS

Accepted Manuscript

This is an *Accepted Manuscript*, which has been through the Royal Society of Chemistry peer review process and has been accepted for publication.

Accepted Manuscripts are published online shortly after acceptance, before technical editing, formatting and proof reading. Using this free service, authors can make their results available to the community, in citable form, before we publish the edited article. We will replace this *Accepted Manuscript* with the edited and formatted *Advance Article* as soon as it is available.

You can find more information about *Accepted Manuscripts* in the Information for Authors.

Please note that technical editing may introduce minor changes to the text and/or graphics, which may alter content. The journal's standard Terms & Conditions and the Ethical guidelines still apply. In no event shall the Royal Society of Chemistry be held responsible for any errors or omissions in this *Accepted Manuscript* or any consequences arising from the use of any information it contains.

ROYAL SOCIETY OF CHEMISTRY

www.rsc.org/jaas

Further investigation into ICP-induced elemental fractionation in LA-ICP-MS using a local aerosol extraction strategy

Tao Luo[a], Yu Wang[a], Zhaochu Hu[a]*, Detlef Günther[a,b]*, Yongsheng Liu[a], Shan Gao[a], Ming Li[a], Shenghong Hu[a]

[a] *State Key Laboratory of Geoprocesses and Mineral Resources, China University of Geosciences, Wuhan, 430074, PR China, (*E-mail: zchu@vip.sina.com)*

[b] *ETH Zurich, Laboratory for Inorganic Chemistry, CH-8093 Zurich, Switzerland, Email:, (*E-mail: guenther@inorg.chem.ethz.ch)*

Submitted to Journal of Analytical Atomic Spectrometry

Abstract

The source and degree of elemental fractionation is one of the remaining challenges in LA-ICP-MS. In this study, the ICP-induced fractionation behavior of 63 elements was studied using a local aerosol extraction strategy while using a 193 nm excimer laser ablation system for sampling. We found that the sampling distance between the ablation site and the gas outlet nozzle tip positively correlated with the size of the laser ablation produced aerosol particles or agglomerates in the local aerosol extraction strategy. Therefore, the local aerosol extraction strategy allowed detailed studies of the ICP-induced fractionation behaviors for different elements. At the low makeup gas flow rate of 0.6 L min^{-1} (hot plasma conditions), the increase in size of aerosol agglomerates or particles because of the increased sampling distance from 1 mm to 10 mm does not affect the ionization efficiency of the sample aerosol in ICP. In contrast, at the high makeup gas flow rate of 0.9 L min^{-1}, the normalized signal intensities of the elements significantly differ when the sampling distance increases from 1 mm to 10 mm. These experimental results suggest that the changes in size of aerosol particles or agglomerates under our given conditions do not affect the transport efficiency of aerosol particles but affect the vaporization of aerosol particles in ICP. The mass load effect is more significant in the presence of large amounts of large aerosol particles and agglomerates, which deteriorates the vaporization of aerosol particles. Our experimental results also show that the sample position in the normal ablation cell affects the size of laser ablation produced aerosol particles or agglomerates. The high velocity of the carrier gas flow rate on the ablation site

facilitates the production of small aerosol agglomerates or particles. To reduce the ICP-induced fractionation behaviors in LA-ICP-MS, hot plasma conditions and high velocity of the carrier gas flow rate on the ablation site are required.

1. Introduction

Since the first application of laser ablation sample introduction with ICP-MS by Gray[1] in 1985, laser ablation inductively coupled plasma mass spectrometry (LA-ICP-MS) has become a powerful technique to directly determine trace elements and isotope ratios in various solid materials[2-12]. The advantages of this technique are rapid throughout, high spatial resolution, little sample size requirements, few sample preparation procedures, reduced water-related spectral interferences and avoidance of the risk of introducing contaminants by conventional chemical digestion.[1-3] However, quantification using non-matrix matched calibration standards is limited by the occurrence of elemental fractionation, which represents the sum of all non-stoichiometric effects that occur during the ablation process, transport and ionization in the ICP source.[13-16]

Elemental fractionation has been one research focus represented in a large number of fundamental studies in LA-ICP-MS.[13, 16-32] It is well known that elemental fractionation is related to the laser wavelength[17-19,33,34], energy density,[20,21] beam diameter[24,25], pulse duration[16,22, 23] and sample matrix[25]. Changing the wavelength from IR to UV and deep UV has successively reduced elemental fractionation.[17-19,33,34] Studies of silicate samples show that smaller mean particle sizes were obtained with decreasing laser wavelengths[19]. Russo et al.[18] reported that wavelength is not the only critical parameter that affects fractionation. Fractionation can be observed for all wavelengths, depending in each case on the laser-beam irradiance and the number of laser pulses at each sample-surface location.[18] Jeong et

al.[20] showed that the size distribution of laser-generated particles changed with the laser power density using a Nd:YAG laser with a wavelength of 266 nm. In the laser power density range of approximately 0.4-0.5 GW/cm^2, the particle size distribution shifts toward fewer large particles.[20] The significantly different laser-induced fractionations between widely used external reference materials NIST SRM 610–614 and natural silicate reference materials at high spatial resolution analysis has been reported by Hu et al.[25] Mank and Mason[28] showed a significant effect of the crater depth-to-diameter ratio (particularly above 6:1) on elemental fractionation. Large diameter craters that are generated under a sufficient power density reduce elemental fractionation effects and produce a higher signal intensities for a longer period of time, which leads to a more accurate and precise analysis.[28] In recent years, studies show that the ablation process using a fs laser is significantly less thermal and leads to a shrinking of the heat-affected zone.[38] The use of femtosecond laser radiation is considered one of the most promising approaches to minimize the elemental fractionation and matrix effects even further.[16, 23, 35-38]

Elemental fractionation has been mainly ascribed to processes that occur at the ablation site in previous works. Recent studies have led to a better understanding of the involved processes, and the focus on laser-sample interaction shifts toward aerosol transport phenomena and the ICP.[29, 39,40-50] Analysis around the ablation crater using SIMS and HR-TEM techniques have further demonstrated that different sized particles produced by laser ablation have different phases and chemical compositions.[50] Because the chemical composition and mineralogy of particles varies

with the particle size, the efficiency of particle transport also plays a role in elemental fractionation.[50] Koch et al.[48] investigated the element ratios in aerosol particles of brass and steel that were produced using a 266 nm Nd:YAG laser. The results implied that the element compositions of the aerosol particles deposited in different parts of the tube deviated from the bulk and varied along the tube. Guillong and Günther[29] indicated that the incomplete aerosol or particle excitation in the ICP was the dominant process that affected elemental fractionation during LA-ICP-MS. Studies of particle size distributions of laser-induced aerosols at 266 nm indicated that the particle size significantly affected the vaporization, atomization and ionization efficiency in the ICP.[29,42] The elemental fractionation in LA-ICP-MS, which is observed at the beginning of a 266 nm single-hole ablation, is predominantly caused by the incomplete vaporization of large particles in the ICP and not dominated by the non-stoichiometric ablation of the glass.[43] When a 193-nm excimer laser generated aerosol was introduced into two different ICP-MS systems, additional observations indicate that the aerosol generated from a single laser source behaves differently in different ICP sources. The measured U/Th ratio differs by a factor of 2 from one instrument to another.[51] Elemental fractionation is reduced by filtering the larger particles from the aerosol that enters the ICP. [29, 42, 43] However, the filtering process produces a 3-fold reduction in the intensity, which indicates that 70% of the transported material was filtered.[29] And stoichiometry of the material is changed by filtering.

These summarized works showed that many parameters affect elemental

fractionation in the ablation process and the ICP, which makes the contributions of the laser and ICP on fractionation relatively difficult to separate. In this study, the fractionation behaviors of 63 elements caused by the plasma related process were investigated using a proposed local aerosol extraction strategy in combination with using different makeup gas flow rates. The mass load-induced matrix effects in the ICP were also studied with the local aerosol extraction strategy. Furthermore, the effects of the sample position in the normal ablation cell on the ICP-induced elemental fractionation in LA-ICP-MS were presented.

Experimental

Instrumentation

Experiments were performed on an Agilent 7500a ICP-MS instrument (Japan) and an excimer 193 nm laser ablation system (Geolas 2005, MicroLas Göttingen, Germany). Details of the instrumental operating conditions and measurement parameters are reported in Table 1. Helium was used as carrier gas in the ablation cell and merged with argon (makeup gas) behind the ablation cell. NIST SRM 610 glass was used for the all of investigations.

Local aerosol extraction strategy

As our previous study described,[52] the standard ablation cell in the GeoLas 2005 system was used, the gas outlet position was changed into the center of the cell using a needle with a nozzle tip (i.d. 0.6 mm) that enabled sampling at the ablation site. The gas inlet nozzle tip (i.d. 2 mm) was directed perpendicular to the bottom of the

ablation cell (Fig. 1). This change in the gas inlet and outlet produced the highest gas velocity at the sampling tip (approximately 10 m s^{-1}), and the gas flow rate decreased with increasing distance from the sampling tip, whereas the gas flow rate distribution in the rest of the cell is notably lower (0.01 m s^{-1}).[52]

In this work, to investigate the ICP-induced elemental fractionation, we kept the carrier gas He constant at flow rate of 0.65 L min^{-1}, then changed the makeup gas flow rates from 0.90 L min^{-1} gradually decrease to 0.60 L min^{-1} by the local aerosol extraction ablation chamber. (Fig. 1) This setup would be perfect for studying ICP related effects because of the carrier gas flow rates have remained through the cell all the time constant and only few or more Ar would have been added right in front of the torch. That means the laser parameter during ablation remain completely constant all the time. We changed the relative position between the ablation site and the outlet extraction nozzle tip between 1 and 10 mm and compared the signal intensities acquired at different distance (from 1 mm to 10 mm).[52] All signals were normalized to the signal intensities acquired at 1 mm distance.

Results and Discussion

ICP-induced element fractionation

Fig. 2 shows the sensitivity enhancement factors in the local aerosol extraction relative to the normal ablation cell. Compared to the normal aerosol extraction, the signal intensities of elements were improved by a factor of 1.1-1.36 using the local aerosol extraction at a short distance of 1 mm between the ablation site and the gas

outlet nozzle tip. The signal enhancement is more significant for volatile elements (B, Cu, Zn, Cd, Ag, Pb and Bi). These volatile elements are enriched in the small particle size fraction of laser-aerosols.[44] The significant enhancement of the signal intensities for volatile elements may be related to the more efficient transportation of small particles using the local aerosol extraction strategy compared to the normal aerosol extraction.

Fig. 3 shows the effects of the distance between the ablation site and the outlet extraction nozzle tip (relative to distance = 1 mm) on the integrated signal intensities for single-hole ablation (spot size: 44 μm) at different makeup gas flow rates of (a) 0.90 L min^{-1}, (b) 0.80 L min^{-1}, (c) 0.70 L min^{-1} and (d) 0.60 L min^{-1}. At the high makeup gas flow rate of 0.9 L min^{-1}, the magnitude of the signal reduction with increasing distance between the ablation site and the outlet nozzle tip varies for different elements. For lithophile elements (Be, Al, Ca, Sc, Y, Zr, Eu, Gd, Tb, Dy, Ho, Er, Tm, Yb, Lu, Hf, Ta and Th), a variation in distance from 1 mm to 10 mm results in a signal reduction of up to ~ 30%. However, the corresponding signal changes of siderophile (P, Cr, Mn, Fe, Co, Ni, Ga, Ge, Mo, W, Au), chalcophile (Cu, Zn, As, Se, Rh, Ag, Cd, In, Sn, Sb, Te, Pt, Tl, Pb, Bi) and some lithophile elements (Li, B, Na, Mg, Si, K, V, Rb, Cs, Ba, U, Ce) were less than 5%. This phenomenon is consistent with a previous study,[52] where the signal changes are attributed to the plume expansion and changes in transport efficiency of different sized particles or aggregates.[52] Larger aerosol particles or aggregates deposit more rapidly because of gravitational effects and are more difficult to push than the smaller aerosol particles when the distance

between the ablation site and the outlet nozzle tip increases. Therefore, it is concluded that lithophile elements [Be, Al, Sc Y, Zr, Nb, REE (excluding Ce), Hf, Ta and Th] are enriched in relatively larger aerosol particles or larger agglomerates, which are significantly lost during the transportation between the ablation site and the outlet nozzle tip. [52] However, as observed in Fig. 3, with decreasing the makeup gas flow rate, the reduction of the normalized signal intensities of refractory lithophile elements (Be, Al, Ca, Sc, Y, Zr, Eu, Gd, Tb, Dy, Ho, Er, Tm, Yb, Lu, Hf, Ta and Th) with increasing sampling distances become smaller. At the makeup gas flow rates of 0.8 L min^{-1}, the normalized signal intensities of refractory lithophile elements show a signal reduction of approximate 20% with the increase in distance from 1 mm to 10 mm. However, at the makeup gas flow rates of 0.6-0.7 L min^{-1}, the normalized signal intensities of all analyzed elements are almost unaffected by the change in sampling distance between the ablation site and the outlet nozzle tip. It is worth noting that the carrier gas flow rate of He is constant at 0.65 L min^{-1} when we change the makeup gas flow rates. Therefore, we are able to demonstrate that the change in sampling distance does not affect the transport efficiency of the different sized particles or aggregates under our given instrument conditions.

As we know, the incomplete conversion of laser-induced aerosols into ions in plasma occurs in the ICP.[29] The effect of the ICP as a possible source of elemental fractionation has recently been studied by many authors.[29,30,39,43,46,47] This ICP-induced elemental fractionation can be reduced when the operating parameters are optimized to generate a sufficient gas temperature in the central channel of the

ICP[43,53]. Generally, a low nebulizer gas flow rate and/or high RF power are facilitated to reduce the ICP-induced elemental fractionation[43,53]. Because the laser ablation condition and the carrier gas flow rate were identical, the observed significant depletion of refractory lithophile elements (Be, Al, Ca, Sc, Y, Zr, Eu, Gd, Tb, Dy, Ho, Er, Tm, Yb, Lu, Hf, Ta and Th) with the increase in sampling distance at higher makeup gas flow rates in Fig. 3 should be attributed to the incomplete vaporization of large particles or aggregates in the ICP.[54] High makeup gas flow rates have a cooling effect on the plasma, which subsequently suppresses the vaporization of the large aerosol particles or aggregates. When the makeup gas flow rate decreases, the central channel of the plasma becomes hotter, and the large aerosol particles or aggregates, which have a longer residence time in the central channel in ICP should evaporate better, which is consistent with the observed phenomenon in Fig. 3 that the depletion of these refractory lithophile elements (Be, Al, Ca, Sc, Y, Zr, Eu, Gd, Tb, Dy, Ho, Er, Tm, Yb, Lu, Hf, Ta and Th) with increasing sampling distance becomes smaller at low makeup gas flow rates.

As illustrated by the modeled gas flow pattern in the ablation cell with the local aerosol extraction strategy using computational fluid dynamics techniques[52], the He carrier gas velocity on the ablation site significantly decreases when the sampling distance between the ablation site and the outlet extraction nozzle tip increases. For example, the He carrier gas velocity is decreased by approximately two orders of magnitude when the sampling distance increases from 1 mm to 5 mm. [52] The observed significant depletion of refractory lithophile elements (Be, Al, Ca, Sc, Y, Zr, Eu, Gd,

Tb, Dy, Ho, Er, Tm, Yb, Lu, Hf, Ta and Th) with the increase in sampling distance at higher makeup gas flow rates (Fig. 3) suggests that the size of the laser ablation produced aerosol particles or aggregates increases when the gas velocity on the ablation site decreases. This finding is important for the design of the laser ablation cell.

Time-dependent elemental fractionation in ICP

As shown in previous publications, for single-hole ablation using a Nd:YAG solid-state laser operating at 266 nm, larger particles occur dominantly during the first 100 laser pulses.[29, 43] To investigate the time-dependent change in size of particles or aggregates and its effect on the ICP-induced elemental fractionation for 193 nm excimer laser ablation, we compared the integrated signal intensities at the 0-20 s and 30-50 s time intervals of laser ablation during single-hole ablation (spot size: 44 μm) under a makeup gas flow rate of 0.80 L min^{-1} (Fig. 4). All signals were normalized to the obtained signal intensities at a sampling distance of 1 mm. For lithophile elements (Be, Al, Ca, Sc, Y, Zr, Eu, Gd, Tb, Dy, Ho, Er, Tm, Yb, Lu, Hf, Ta and Th), a variation in distance from 1 mm to 10 mm results in a normalized signal suppression of approximately 30% in the first 20 s of ablation (Fig. 4), which is mainly caused by the incomplete vaporization of larger aerosol particles in the ICP. In contrast, the corresponding normalized signal is almost unaffected in the period of 30-50 s when the distance between the ablation site and the outlet nozzle tip changes from 1 mm to 10 mm (Fig. 4). These differences indicate a time-dependent particle size distribution

during single-hole ablation. Similar to the 266 nm laser ablation, larger particles or aggregates also appear when 193 nm is used for ablation and are dominantly generated at the beginning of the ablation.

Fig. 5 shows the calculated elemental fractionation indices (FIs) for 63 isotopes from ablation of NIST 610 using a normal ablation cell at a crater diameter of 16 μm, which represents laser ablation-dominated fractionation, and the local aerosol extraction strategy at a sampling distance of 10 mm at a crater diameter of 160 μm under makeup gas flow rate of 0.90 L min^{-1}, which represents the ICP-induced fractionation. The FIs for 63 isotopes were calculated based on Ca as the internal standard, and the 50 s transient signals were divided into equal time intervals instead of 240 s as reported by Fryer[55]. As shown in Fig. 5, good complement exists between the calculated FIs dominated by the plasma and laser- ablation related processes. This good complement suggests that both laser ablation and plasma-related fractionation effects are controlled by the same elemental properties. Several studies were performed to correlate the physical properties of elements with the degree of laser ablation-induced elemental fractionation (e.g., boiling points, melting points, ionization potential, condensation temperature, ionic radius, field strength，the sum of the first and second ionization enthalpies)[9, 56-60] Fig. 6 shows that the 50% condensation temperatures[61] and normalized signal intensity using the local aerosol extraction strategy (as shown in Fig. 3) are complementary. Elements with higher condensation temperatures tend to have a larger depletion with increasing sampling distances from the ablation site. Elements with lower condensation temperatures show

no depletion. In combination with the results in Fig. 5, this correlation can certainly show that both laser- and ICP-induced elemental fractionations are closely related to 50% condensation temperatures.

Large aerosol particles or aggregates induce mass load effects in the ICP

To describe the processes in the plasma in detail, U and Th were often used as indicators because of their notably similar ionization potentials (U: 597.6, Th: 587 kJ mol^{-1}), mass number and their almost identical concentrations in the NIST 610 (U=462.9 μg g^{-1}, Th=463.1 μg g^{-1})[29,51,62]. Fig. 7 shows the U/Th ratios during single-hole ablation with different crater diameters under various makeup gas flow rates using the local aerosol extraction. To produce large particles or agglomerates, the relative position between the ablation site and the outlet extraction nozzle tip was fixed at 10 mm. As shown in Fig. 7, at the relatively higher makeup gas flow rates of 1.0 and 0.9 L min^{-1}, the U/Th ratio sharply increases to a notably high value at the beginning of the ablation for large spot sizes of 90-160 μm; then, it gradually decreases to a steady value after 20 s of ablation. This type of U/Th ratio change is not significant for small spot sizes of 16-32 μm. Our previous results indicate that the larger particles or aggregates are dominantly generated at the beginning of the ablation for a 193 nm laser. Therefore, the significantly increased U/Th ratio at the beginning of the ablation should be attributed to the incomplete vaporization of large aerosol particles. The elemental ratio of U/Th decreases from 3.8 to approximately 2.3 when the crater diameter decreases from 160 μm to 16 μm at the beginning of the

ablation with a makeup gas flow rate of 1.0 L min^{-1}. The particle size distribution measurements for different crater sizes show that the particle size distribution does not depend on the crater diameter for the ablation at 193 nm.[24, 47] Thus, the reduced U/Th ratio with decreasing crater diameter at the beginning of the ablation cannot be attributed to the change in particle size distribution. This result clearly indicates that the mass load significantly affects the vaporization of aerosol particles. A lower mass load corresponds to better aerosol particle vaporization in the ICP. When the makeup gas flow rate decreases from 1 L min^{-1} to 0.7 L min^{-1}, the integrated U/Th ratios are significantly reduced, and the variation of U/Th ratios during single-hole ablation at large spot sizes disappears. It is clear that a hot plasma condition is essential for the alleviation of the mass load effect in the ICP.

Effect of sample position in the ablation cell on the ICP-induced elemental fractionation

The sampling position effect in the ablation cell is a well-known phenomenon in LA-ICP-MS analysis.[63-65] Our study illustrates that the He gas velocity on the laser ablation site significantly affects the size of the laser ablation produced aerosol particles or aggregates. Because the velocity of the carrier gas in the ablation chamber significantly varies with different positions,[52, 63, 65, 66] we believe that this change may be an important source of element fractionation at different sampling positions. Fig. 8 shows the normalized signal intensities for 63 investigated elements at various makeup gas flow rates using the normal ablation cell. The obtained signals at position

B were normalized to the obtained signal intensities at position A. At a higher makeup gas flow rate of 1.0 L min^{-1}, the normalized signal intensities for the refractory lithophile elements (Be, Al, Ca, Sc, Y, Zr, Eu, Gd, Tb, Dy, Ho, Er, Tm, Yb, Lu, Hf, Ta and Th) are only approximately 0.55-0.70. In contrast, the normalized signal intensities for all investigated elements are approximately 1 at a lower makeup gas flow rate of 0.7 L min^{-1}. This result suggests that the transport efficiency of the produced aerosol particles or aggregates is similar for both positions A and B. These relative signal intensity variations between positions A and B at different makeup gas flow rates are similar to those observed for the local aerosol extraction strategy at various makeup gas flow rates. The He flow rate varies from point to point in the ablation chamber in this study. The carrier gas velocity is approximately 9.0 m s^{-1} at position A, which decreases to a notably low value of 0.2 m s^{-1} at position B.[52] As we previously discussed, the carrier gas velocity on the ablation site has a negative correlation with the size of the produced aerosol particles or aggregates. Thus, the significantly reduced normalized signal intensity (position B normalized to position A) for the refractory lithophile elements (Be, Al, Ca, Sc, Y, Zr, Eu, Gd, Tb, Dy, Ho, Er, Tm, Yb, Lu, Hf, Ta and Th) at a higher makeup gas flow rate of 1.0 L min^{-1} in Fig. 8 should be attributed to the incomplete vaporization of large aerosol particles or aggregates in the ICP. Loewen et al.[65] investigated elemental fractionation in silicate glasses using single-volume and two-volume ablation chambers. Their results show that this fractionation is unrelated to the interaction between the laser pulse and the solid material during progressive ablation but does correlate with the local He velocity

at the position of analysis.[65] Our results suggest that the differential responses of volatile and refractory elements relative to ^{43}Ca for different analysis locations in a single-volume ablation chamber observed by Loewen[65] are related to the ICP-induced elemental fractionation because the laser ablation produced particle or aggregate size changes at different analysis locations. This result reinforces the importance of a hot plasma condition for LA-ICP-MS analysis.

Conclusions

Our work indicates that the ablation location-related gas flow rate in the ablation chamber significantly affects the size of laser ablation produced aerosol particles or agglomerates. Larger aerosol particles or aggregates are produced in the low-He velocity zones of the ablation cell. These large particles or aggregates cannot be completely vaporized in the ICP. This type of ICP-induced elemental fractionation results in significant depletion of refractory elements (Be, Al, Ca, Sc, Y, Zr, Eu, Gd, Tb, Dy, Ho, Er, Tm, Yb, Lu, Hf, Ta and Th). It is also shown that the mass load induced matrix effect is more significant in the presence of large amounts of larger aerosol particles and that this type of matrix effect severely degrades the vaporization of large aerosol particles or aggregates in the ICP. To minimize the particle or aggregate size-related elemental fractionation in the ICP, a high velocity of the carrier gas on the ablation site and hot plasma conditions are required.

Acknowledgements

We would like to thank Mary MacLeod and anonymous reviewers for their constructive comments. This research is supported by the National Nature Science Foundation of China (Grants 41273030, 41322023, and 41373026), the Fundamental Research Funds for National Universities, the CERS-China Equipment and Education Resources System (CERS-1-81), the State Administration of the Foreign Experts Affairs of China (B07039), and the MOST Special Fund from the State Key Laboratories of Geological Processes and Mineral Resources.

References

1. A. L. Gray, *Analyst*, 1985, **110**, 551-556.
2. K. E. Jarvis and J. G. Williams, *Chem. Geol.*, 1993, **106**, 251-262.
3. S. F. Durrant and N. I. Ward, *J. Anal. At. Spectrom.*, 2005, **20**, 821-829.
4. J. S. Becker, M. Zoriy, J. S. Becker, J. Dobrowolska and A. Matusch, *J. Anal. At. Spectrom.*, 2007, **22**, 736-744.
5. T. Trejos and J. R. Almirall, *Talanta*, 2005, **67**, 388-395.
6. L. Xu, Z. C. Hu, W. Zhang, L. Yang, Y. S. Liu, S. Gao, T. Luo and S. H. Hu, *J. Anal. At. Spectrom.*, 2015, **30**, 232-244.
7. Z. C. Hu, W. Zhang, Y. S. Liu, S. Gao, M. Li, K.Q. Zong, H. H. Chen and S. H. Hu, *Anal. Chem.*, 2015, **87**, 1152–1157.
8. S. E. Gilbert, L. V. Danyushevsky, T. Rodemann, N. Shimizu, A. Gurenko, S. Meffre, H. Thomas, R. R. Large and D. Death, *J. Anal. At. Spectrom.*, 2014, **29**, 1042-1051.
9. R. W. Nesbitt, T. Hirata, I. B. Butler and J. A. Milton, *Geostand. Newsl.*, 1997, **21**, 231-243.
10. N. Mokgalaka and J. Gardea‐Torresdey, *Appl. Spectrosc. Rev.*, 2006, **41**, 131-150.
11. J. S. Becker, A. Matusch and B. Wu, *Anal. Chim. Acta.*, 2014, **835**, 1-18.
12. I. Horn, R. L. Rudnick and W. F. McDonough, *Chem. Geol.*, 2000, **164**, 281–301.
13. H. Longerich, D. Günther and S. Jackson, *Fresen. J. Anal. Chem.*, 1996, **355**, 538-542.
14. D. Günther and B. Hattendorf, *Trend. Anal. Chem.*,2005, **24**, 255-265.
15. C. C. Garcia, H. Lindner and K. Niemax, *J. Anal. At. Spectrom.*, 2009, **24**, 14-26. 16. F. Claverie, B. Fernández, C. Pécheyran, J. Alexis and O. F. Donard, *J. Anal. At. Spectrom.*, 2009, **24**, 891-902.
17. T. Jeffries, S. Jackson and H. Longerich, *J. Anal. At. Spectrom.*, 1998, **13**, 935-940.
18. R. Russo, X. Mao, O. Borisov and H. Liu, *J. Anal. At. Spectrom.*, 2000, **15**, 1115-1120.
19. M. Guillong, I. Horn and D. Günther, *J. Anal. At. Spectrom.*, 2003, **18**, 1224-1230.
20. S. Jeong, O. Borisov, J. Yoo, X. Mao and R. Russo, *Anal. Chem.*, 1999, **71**, 5123-5130.
21. I. Horn, M. Guillong and D. Günther, *Appl. Surf. Sci.*, 2001, **182**, 91-102.
22. R. E. Russo, X. Mao, J. J. Gonzalez and S. S. Mao, *J. Anal. At. Spectrom.*, 2002, **17**, 1072-1075.
23. J. Koch, A. Von Bohlen, R. Hergenröder and K. Niemax, *J. Anal. At. Spectrom.*, 2004, **19**, 267-272.
24. H.R. Kuhn and D. Günther, *J. Anal. At. Spectrom.*, 2006, **21**, 1209-1213.
25. Z. C. Hu, Y. S. Liu, L. Chen, L. Zhou, M. Li, K. Q. Zong, L. Y. Zhu and S. Gao, *J. Anal. At. Spectrom.*, 2011, **26**, 425-430.
26. I. Horn and D. Günther, *Appl. Surf. Sci.*, 2003, **207**, 144-157.
27. S. Eggins, L. Kinsley and J. Shelley, *Appl. Surf. Sci.*, 1998, **127**, 278-286.
28. A. J. Mank and P. R. Mason, *J. Anal. At. Spectrom.*, 1999, **14**, 1143-1153.
29. M. Guillong and D. Günther, *J. Anal. At. Spectrom.*, 2002, **17**, 831-837.
30. H. R. Kuhn and D. Günther, *Anal. Chem.*, 2003, **75**, 747-753.
31. P. Outridge, W. Doherty and D. Gregoire, *Spectrochim. Acta, Part B.*, 1997, **52**, 2093-2102.
32. S. Chenery and J. M. Cook, *J. Anal. At. Spectrom.*, 1993, **8**, 299-303.
33. D. Günther, R. Frischknecht, C. A. Heinrich and H.-J. Kahlert, *J. Anal. At. Spectrom.*, 1997, **12**,

939-944.
34. D. Günther, I. Horn and B. Hattendorf, *Fresen. J. Anal. Chem.*, 2000, **368**, 4-14.
35. R. Hergenröder, O. Samek and V. Hommes, *Mass. spectrom. rev.*, 2006, **25**, 551-572.
36. F. Poitrasson, X. Mao, S. S. Mao, R. Freydier and R. E. Russo, *Anal. Chem.*, 2003, **75**, 6184-6190.
37. I. Horn and F. von Blanckenburg, *Spectrochim. Acta, Part B.*, 2007, **62**, 410-422.
38. B. Fernández, F. Claverie, C. Pécheyran, O. F. Donard and F. Claverie, *Trac. Trend. Anal. Chem.*, 2007, **26**, 951-966.
39. D. B. Aeschliman, S. J. Bajic, D. P. Baldwin and R. Houk, *J. Anal. At. Spectrom.*, 2003, **18**, 1008-1014.
40. I. Rodushkin, M. D. Axelsson, D. Malinovsky and D. C. Baxter, *J. Anal. At. Spectrom.*, 2002, **17**, 1223-1230.
41. I. Rodushkin, M. D. Axelsson, D. Malinovsky and D. C. Baxter, *J. Anal. At. Spectrom.*, 2002, **17**, 1231-1239.
42. M. Guillong, H.-R. Kuhn and D. Günther, *Spectrochim. Acta, Part B.*, 2003, **58**, 211-220.
43. H. R. Kuhn, M. Guillong and D. Günther, *Anal. bioanal. chem.*, 2004, **378**, 1069-1074.
44. H. R. Kuhn and D. Günther, *J. Anal. At. Spectrom.*, 2004, **19**, 1158-1164.
45. J. Koch, M. Wälle, J. Pisonero and D. Günther, *J. Anal. At. Spectrom.*, 2006, **21**, 932-940.
46. Z. K. Wang, B. Hattendorf and D. Günther, *J. Anal. At. Spectrom.*, 2006, **21**, 1143-1151.
47. I. Kroslakova and D. Günther, *J. Anal. At. Spectrom.*, 2007, **22**, 51-62.
48. J. Koch, I. Feldmann, N. Jakubowski and K. Niemax, *Spectrochim. Acta, Part B.*, 2002, **57**, 975-985.
49. D. Fliegel and D. Günther, *Spectrochim. Acta, Part B.*, 2006, **61**, 841-849.
50. J. Košler, M. Wiedenbeck, R. Wirth, J. Hovorka, P. Sylvester and J. Míková, *Spectrochim. Acta, Part B.*, 2005, **20**, 402-409.
51. D. Günther, *Anal. bioanal. chem.*, 2002, **372**, 31-32.
52. Z. C. Hu, Y. S. Liu, S. Gao, S. H. Hu, R. Dietiker and D. Günther, *J. Anal. At. Spectrom.*, 2008, **23**, 1192-1203.
53. B. Hattendorf, C. Latkoczy and D. Günther, *Anal. Chem.*, 2003, **75**, 341 A-347 A.
54. L. Flamigni, J. Koch, H. Wiltsche, R. Brogioli, S. Gschwind and D. Günther, *J. Anal. At. Spectrom.*, 2012, **27**, 619-625.
55. B. J. Fryer, S. E. Jackson and H. P. Longerich, *Can. Mineral.*, 1995, **33**, 303-303.
56. T. E. Jeffries, N. J. Pearce, W. T. Perkins and A. Raith, *Anal. Commun.*, 1996, **33**, 35-39.
57. P. Outridge, W. Doherty and D. Gregoire, *Spectrochim. Acta, Part B.*, 1996, **51**, 1451-1462.
58. H.C. Liu, O. V. Borisov, X. Mao, S. Shuttleworth and R. E. Russo, *Appl. Spectrosc.*, 2000, **54**, 1435-1442.
59. M. Motelica-Heino, P. Le Coustumer and O. Donard, *J. Anal. At. Spectrom.*, 2001, **16**, 542-550.
60. Z. X. Chen, *J. Anal. At. Spectrom.*, 1999, **14**, 1823-1828.
61. K. Lodders, *Astrophys. J.*, 2003, **591**, 1220.
62. Z. K Wang, B. Hattendorf and D. Günther, *J. Am. Soc. Mass Spectr.*, 2006, **17**, 641-651. 63. D. Bleiner and D. Günther, *J. Anal. At. Spectrom.*, 2001, **16**, 449-456.
64. D. Bleiner and Z. X. Chen, *Laser Ablation ICP–MS in the Earth Sciences: Current Practices and Outstanding Issues (P. Sylvester, ed.). Mineral. Assoc. Can. Short Course Series*, 2008, **40**, 35-52.
65. M. W. Loewen and A. J. Kent, *J. Anal. At. Spectrom.*, 2012, **27**, 1502-1508.
66. D. Bleiner and A. Bogaerts, *Spectrochim. Acta, Part B.*, 2007, **62**, 155-168.

Table 1 Summary of the operating conditions for LA-ICP-MS measurements.

GeoLas Laser ablation system	
Wavelength	193 nm, Excimer laser
Repetition rate	8 Hz
Pulse length	15 ns
Energy density	10 J cm^{-2}
Spot sizes	16, 32,44, 60, 90 and 160 µm
Sample	NIST SRM 610
Ablation cell gas	Helium (0.65 L min^{-1})
Makeup gas	Argon (1.0, 0.90, 0.85, 0.80, 0.70 and 0.60 L min^{-1})
Agilent 7500a ICP-MS	
RF power	1350 W
Plasma gas flow rate	14.0 l min^{-1}
Auxiliary gas flow rate	1.0 l min^{-1}
Sampling depth	5.0 mm
Ion optic settings	Typical
Isotopes measured	^{7}Li, ^{9}Be, ^{11}B, ^{23}Na, ^{25}Mg, ^{27}Al, ^{29}Si, ^{31}P, ^{39}K, ^{42}Ca, ^{45}Sc, ^{49}Ti, ^{51}V, ^{52}Cr, ^{55}Mn, ^{57}Fe, ^{59}Co, ^{60}Ni, ^{65}Cu, ^{66}Zn, ^{71}Ga, ^{72}Ge, ^{75}As, ^{82}Se, ^{85}Rb, ^{88}Sr, ^{89}Y, ^{90}Zr, ^{93}Nb, ^{95}Mo, ^{103}Rh, ^{107}Ag, ^{111}Cd, ^{115}In, ^{118}Sn, ^{121}Sb, ^{126}Te, ^{133}Cs, ^{137}Ba, ^{139}La, ^{140}Ce, ^{141}Pr, ^{143}Nd, ^{147}Sm, ^{151}Eu, ^{157}Gd, ^{159}Tb, ^{163}Dy, ^{165}Ho, ^{166}Er, ^{169}Tm, ^{173}Yb, ^{175}Lu,^{179}Hf, ^{181}Ta, ^{182}W, ^{195}Pt, ^{197}Au, ^{205}Tl, ^{208}Pb, ^{209}Bi, ^{232}Th, ^{238}U
Dwell time per isotope	10 ms
Detector mode	Dual

Figure captions

Fig. 1 Schematic drawing of the experiment: (a) the normal ablation chamber; (b) the local aerosol extraction ablation chamber; (c) the schematic set-up of the laser ablation ICP-MS system used in this study.

Fig. 2 Sensitivity enhancement factors in the local aerosol extraction (at distance=1 mm) relative to the normal ablation cell.

Fig. 3 Effects of the distance between the ablation site and the outlet extraction nozzle tip on the integrated signal intensities (50 s) (relative to distance=1 mm) for single-hole ablation (spot size: 44 μm) at various makeup flow rates (a: 0.9 L min^{-1}; b: 0.8 L min^{-1}; c: 0.7 L min^{-1}; d: 0.6 L min^{-1}).

Fig. 4 Effects of the distance between the ablation site and the outlet extraction nozzle tip on the integrated signal intensities of different integrated time intervals (a: 0-20 s; b: 30-50 s) for single-hole ablation (spot size: 44 μm) at the makeup flow rate of 0.8 L min^{-1}.

Fig. 5 Calculated elemental fractionation indices (FIs) for 63 isotopes from ablation of NIST 610 using a normal ablation cell at a crater diameter of 16 μm and the local aerosol extraction strategy at a distance of 10 mm at a crater diameter of 160 μm with

a makeup gas flow rate of 0.90 L min^{-1}.

Fig. 6 Relationship between the 50% condensation temperatures[58] and the normalized signal intensity using local aerosol extraction strategy.

Fig. 7 U/Th ratios for single-hole ablation of NIST 610 with different crater diameters at various makeup gas flow rates (a: 1.0 L min^{-1}; b: 0.9 L min^{-1}; c: 0.8 L min^{-1}; d: 0.7 L min^{-1}) using the local aerosol extraction strategy at distance=10 mm.

Fig. 8 Relative signal intensities at different analysis locations (position A and position B) at various makeup gas flow rates using the normal ablation cell. The signals acquired at position B were normalized to the signal intensities acquired at position A.

Fig. 1

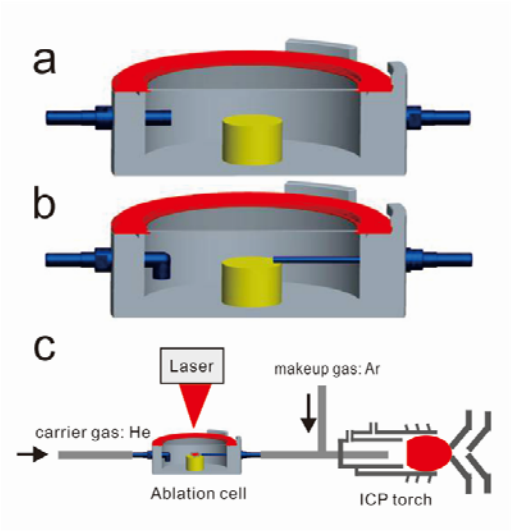

Fig. 2

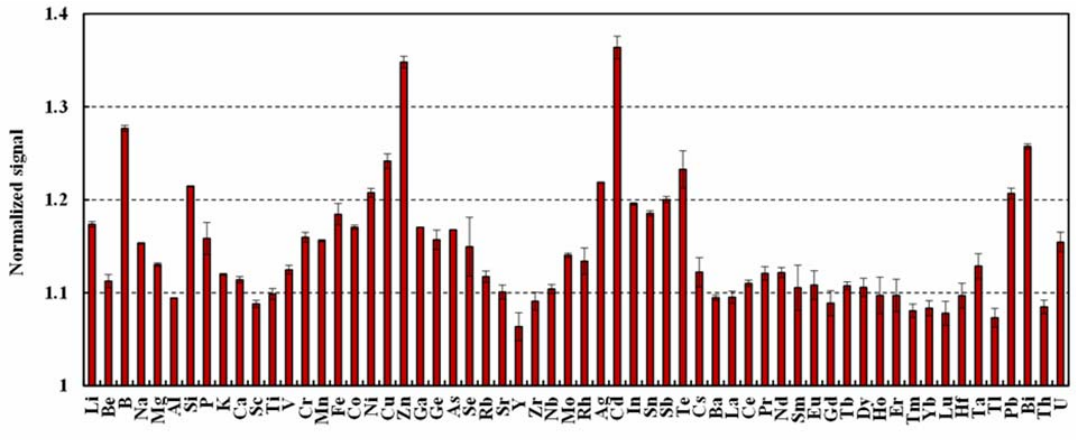

Fig. 3

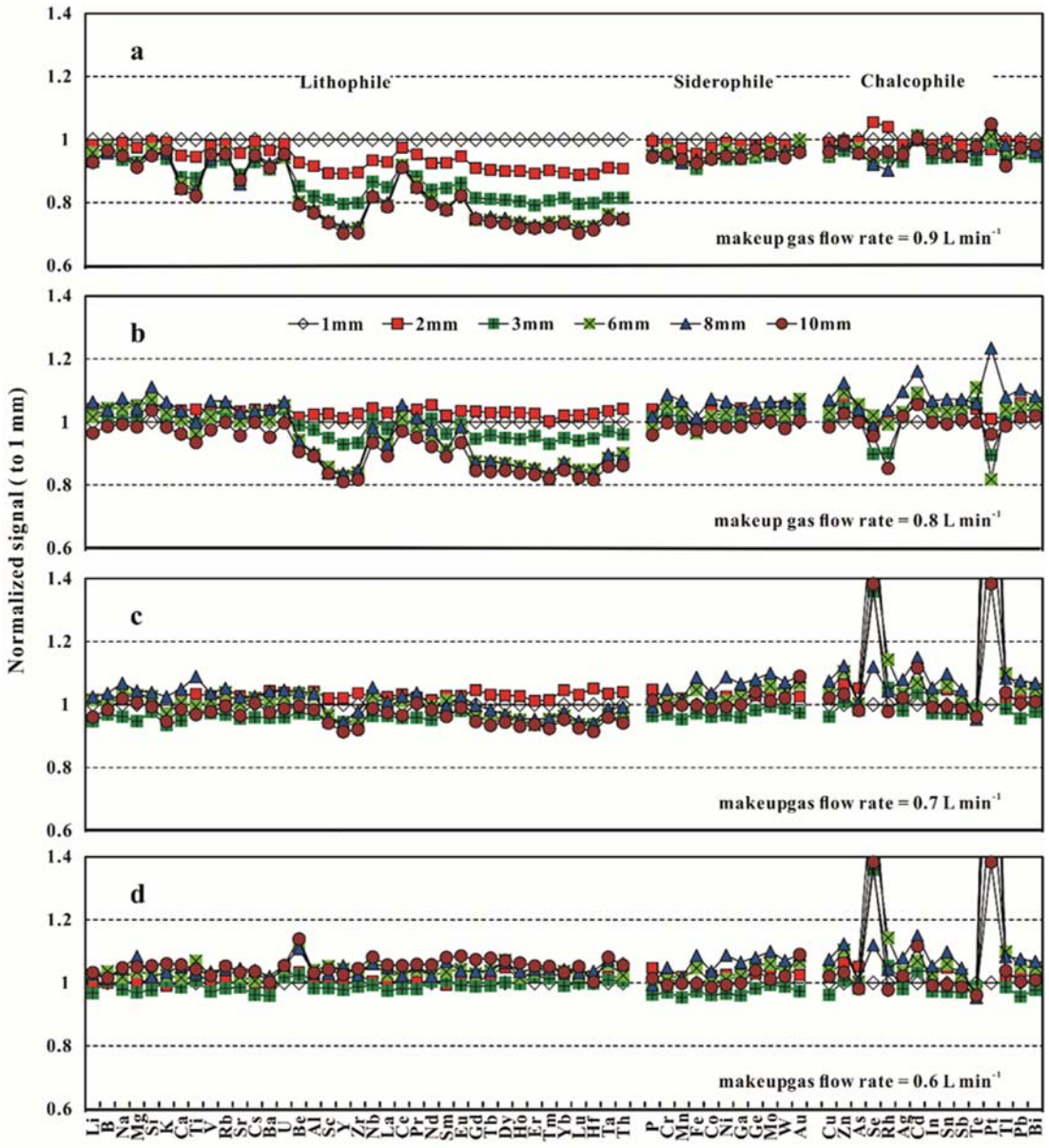

Fig. 4

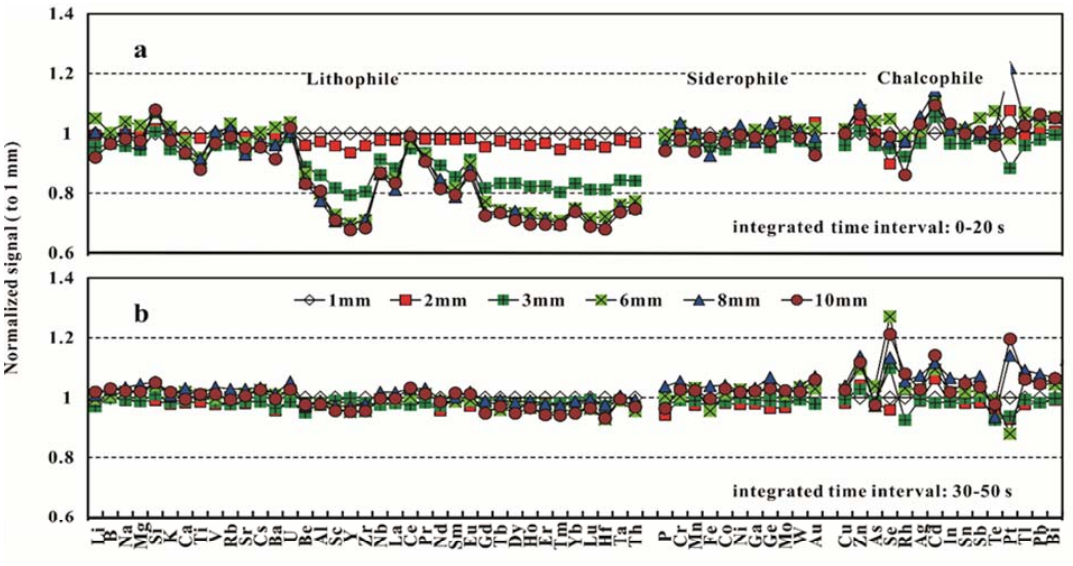

Fig. 5

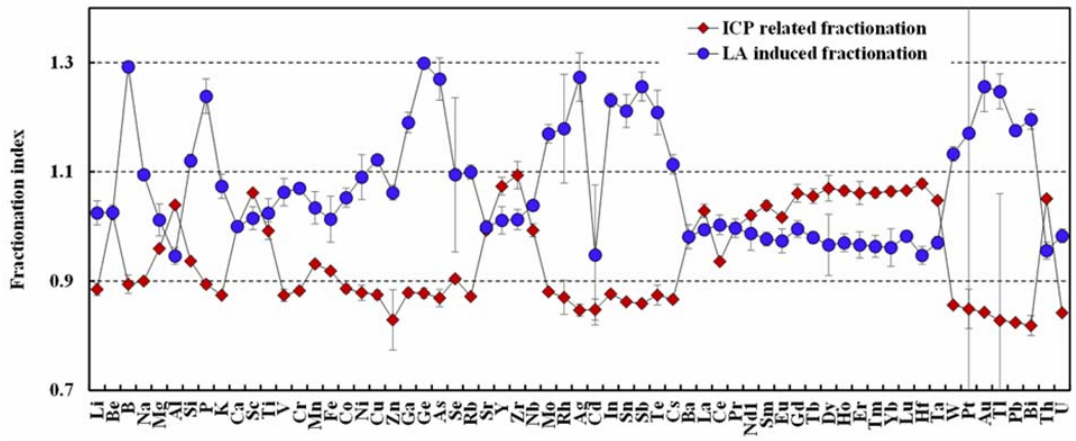

Fig. 6

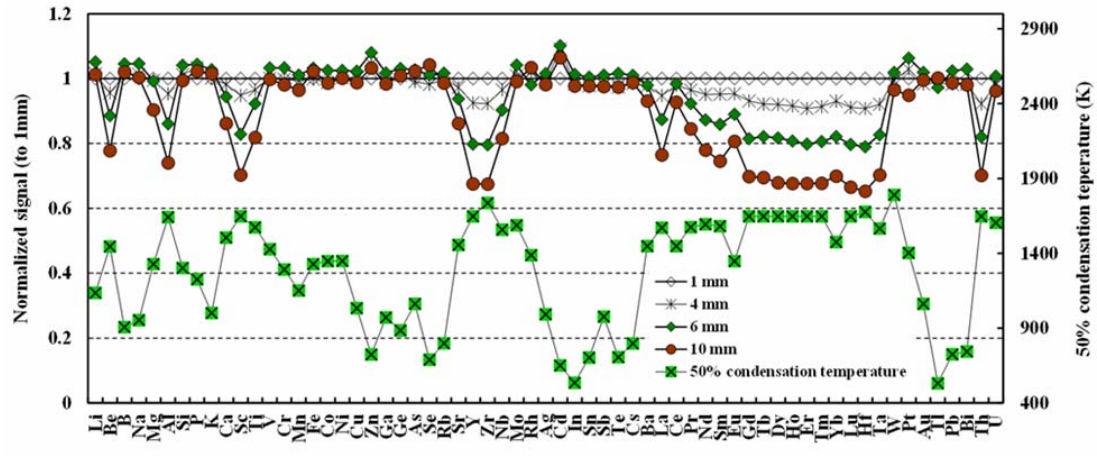

Fig. 7

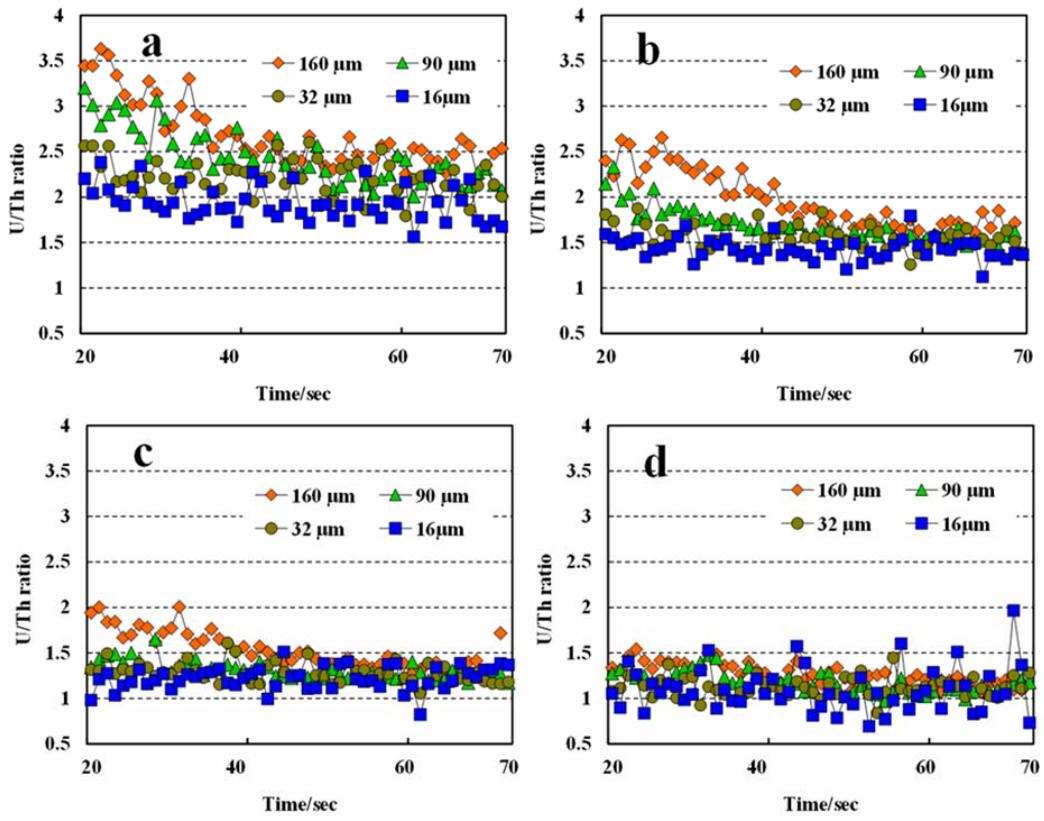

Fig. 8